Progress In Electromagnetics Research M, Vol. 48, 67–76, 2016

Highly Coherent Supercontinuum Generation in the Normal Dispersion Liquid-Core Photonic Crystal Fiber

Zheng Guo*, Jinhui Yuan, Chongxiu Yu, Xinzhu Sang, Kuiru Wang, Binbin Yan, Lixiao Li, Shuai Kang, and Xue Kang

Abstract—In this paper, a liquid-core photonic crystal fiber (LCPCF) with small hollow-core filled by chalcogenide material CS_2 is designed. The supercontinuum (SC) generation in such a LCPCF with nonlinear coefficient of $3327\,W^{-1}\cdot km^{-1}$ at 1550 nm and wide normal dispersion regime spanning from 1200 to 2500 nm is numerically studied by solving the generalized nonlinear Schrödinger equation. The influences of the pump pulse parameters on the SC spectral width and coherence are demonstrated, and the optimum pump condition for the SC generation is determined. Our study work can provide an alternative way for obtaining highly coherent SC, which is important for the applications in optical coherence tomography, frequency combs, and ultrashort pulse generation.

1. INTRODUCTION

Supercontinuum (SC) generation in optical waveguide has become an active research because its enormous applications in wavelength division multiplexing, optical frequency combs, optical coherence tomography, and frequency metrology [1–7]. The spectral broadening results from the interplay between group-velocity dispersion (GVD) and a series of nonlinear effects. The physical mechanism of SC generation in the anomalous dispersion region of optical waveguide is dominated by the soliton fission and dispersive waves [8]. Lot of studies demonstrate that SC spanning more than one octave can be easily obtained when the pump wavelengths of femtosecond or picosecond pulses are in anomalous dispersion regime and close to the zero-dispersion wavelength (ZDW) of optical waveguide. Ranka et al. showed the SC spanning over an octave from 400 to 1500 nm using only 75 cm PCF with the ZDWs within the range of $765 \sim 775$ nm [9]. Omenetto et al. reported the SC from 350 nm to 3 μm in sub-centimeter lengths of soft-glass photonic crystal fibers (PCFs) with a ZDW at 1300 nm [10]. Qin et al. used a 2.5-cm-long fluoride fiber with ZDW at 1650 nm to generate SC from UV ($\sim$ 350 nm) to 3.85 μm [11]. However, the solitonic dynamics are very sensitive to the pump pulse fluctuation and pulse shot noise [12, 13], so the coherence of the SC generated could be degraded severely. Recently, the SC generation in normal dispersion regime of the optical waveguide has attracted great interest. Hooper et al. used 1 m PCF with all-normal GVD to generate 800 nm bandwidth continuum [14]. Li et al. numerically investigated the SC generation in PCFs with all-normal GVD, and discussed the physical mechanism and coherence of generated SC [15]. Yan et al. showed the simulation result of 2–5 μm SC generation in an As_2S_3 PCF with all-normal flat dispersion profile [16]. Because the spectral broadening is mainly attributed to self-phase modulation (SPM) and stimulated Raman scattering (SRS) [8], the related problems existing in the solitonic dynamics can be avoided [17]. But for the highly coherent SC in normal dispersion regime, higher pump power, shorter pulse duration, and longer waveguide length are needed. In order to avoid these problems, the use of highly nonlinear optical waveguides is necessary.

Received 23 December 2015, Accepted 16 April 2016, Scheduled 2 May 2016

* Corresponding author: Zheng Guo (huberyace_guo@163.com).

The authors are with the State Key Laboratory of Information Photonics and Optical Communications, Beijing University of Posts and Telecommunications, P. O. Box 163 (BUPT), Beijing 100876, China.

In the past decades, the silica photonic crystal fibers (PCFs) are demonstrated to be an ideal medium for SC generation because of its adjustable dispersion and enhanced nonlinearity [18, 19]. But the low nonlinear-index and strong absorption in mid-infrared region have a great limit. Recently, liquid-core PCFs (LCPCFs), whose cores are filled with highly nonlinear liquid materials, have been proposed for SC generation. Bozolan et al. used a 5-cm-long water-core PCF to achieve a 500-nm spectrum broadening [20]. Zhang et al. studied the optical properties of hollow-core PCF filled with highly nonlinear liquid chloroform and investigated the SC generation [21]. Among these liquid materials, CS_2 is a good candidate because of its large nonlinear-index and good mid-infrared transparency. Several studies reported the SC generation in the anomalous dispersion regime of hollow-core fibers filled with CS_2 [22–24]. In this paper, LCPCF with high nonlinear coefficient and wide normal dispersion regime is proposed, then the SC generation in designed LCPCF is numerically studied and discussed. The optimum pump condition for the SC generation is determined through studying the influences of the pump pulse parameters on the SC spectral width and coherence.

2. DESIGN OF LCPCF AND THEORY MODEL

In this section, we will design and optimize fiber structures by the full-vector finite element method which is widely used for analyzing the optical waveguide. The cross-section of the designed LCPCF is shown in Fig. 1, where small hollow-core is filled with CS_2 (red circle), and the substrate is the silica material (grey area). The four rings of air holes (white holes) are arranged in a hexagonal lattice to adjust the dispersion profile and ensure sufficiently low confinement loss. As reported in [24–26], this kind of fiber can be easily fabricated by infusing the liquid into a small hollow-core PCF.

The effective refractive index of CS_2 is obtained from [22],

$$n_{CS_2}(\lambda) = 1.580826 + 1.52389 \cdot 10^{-2}/\lambda^2 + 4.8578 \cdot 10^{-4}/\lambda^4 - 8.2863 \cdot 10^{-5}/\lambda^6 + 1.4619 \cdot 10^{-5}/\lambda^8 \quad (1)$$

The GVD is given by

$$D = -\frac{\lambda}{c}\frac{d^2\mathrm{Re}(n_{eff})}{d\lambda^2} \quad (2)$$

where c is the speed of light in vacuum, and $\mathrm{Re}(n_{eff})$ stands for the real part of the effective refractive indices.

The dispersion profiles of the LCPCF can be evidently affected by the ratio of hole diameter (d) and pitch (Λ). In this study, we fix $d = 1.8\,\mu\mathrm{m}$ and adjust Λ so as to obtain the desired dispersion curve. Fig. 2 shows the calculated GVD profiles when Λ is changed from 2 to 5 μm. When $\Lambda = 2.0\,\mu\mathrm{m}$,

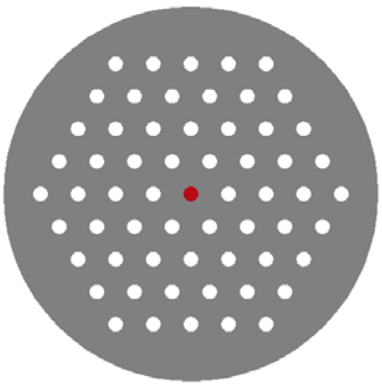

Figure 1. Cross-section of the proposed LCPCF.

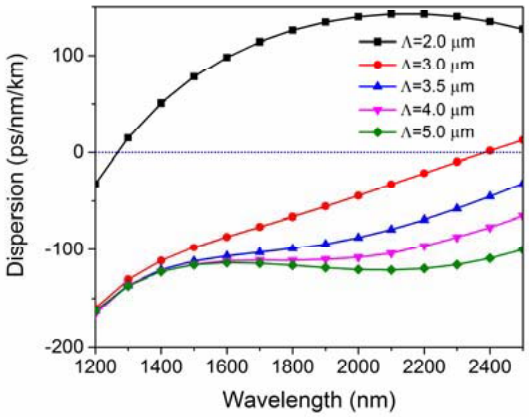

Figure 2. GVD curves of LCPCFs with different pitches.

fiber has anomalous dispersion from 1270 to 2500 nm. With the increases of Λ, the first zero-dispersion wavelength of the proposed fiber moves towards longer wavelengths gradually. The main reason is considered that the effect of waveguide dispersion decreases, and the material dispersion dominates. When $\Lambda \geq 3.5\,\mu$m, the LCPCF has an all normal dispersion which is necessary for our research within the wavelength range of 1200 to 2500 nm. On the other hand, the values of D and dispersion slope decrease as Λ increases at 1550 nm. It can be seen from Fig. 2 that when $\Lambda = 5\,\mu$m, the value of D at 1550 nm is as large as -114.26 ps/km/nm, which can strongly suppress the modulation instability during the SC generation. The dispersion slope at 1550 nm is only 0.021 ps/km/nm^2, and the effect of third-order dispersion is small. Thus, the fiber parameters are chosen as following: $d = 1.8\,\mu$m, and $\Lambda = 5\,\mu$m.

Next, the CS_2 is filled into the hollow-hole to achieve high nonlinearity. The nonlinear coefficient γ is expressed as

$$\gamma = \frac{2\pi \iint n_2(x,y)\,|E(x,y)|^4 dxdy}{\lambda \left| \iint |E(x,y)|^2\, dxdy \right|^2} \tag{3}$$

$$n_2(x,y) = \begin{cases} 2.7 \times 10^{-18} & \text{core} \\ 2.48 \times 10^{-20} & \text{cladding} \end{cases} \tag{4}$$

where $E(x,y)$ is the transverse distribution of electric field of fundamental mode and $n_2(x,y)$ the nonlinear index of CS_2 [23] and silica material. The calculation result shows that this fiber has the γ value of 3327 W^{-1}·km^{-1} at 1550 nm.

Finally, the propagation dynamic of the short pulses inside the LCPCF with normal dispersion can be simulated by solving the generalized nonlinear Schrodinger equation with Runge-Kutta algorithm [27],

$$\begin{aligned} \frac{\partial A}{\partial z} &= -\frac{\alpha}{2}A - \left(\sum_{k\geq 2} \beta_n \frac{i^{n-1}}{n!} \frac{\partial^n}{\partial T^n} \right) A \\ &\quad + i\gamma \frac{1}{\omega_0} \left(1 + \frac{\partial}{\partial T} \right) \times \left((1 - f_R)\, A|A|^2 + f_R A \int_0^\infty h_R(t)\, |A(z, T-t)|^2\, dt \right) \end{aligned} \tag{5}$$

where $A = A(z,t)$ is the envelope of the electric field, α the propagation loss, β_n the nth order GVD coefficient at the center frequency ω, γ the nonlinear coefficient, and f_R and $h_R(t)$ represent the Raman contribution and Raman response function of CS_2, respectively.

Because of nonexistent confinement loss of the proposed structure and very small absorption loss of CS_2 in the near-infrared region [24], the propagation loss of the LCPCF with only tens of centimeters can be neglected. The dispersion order considered is up to 13 in our simulation, and the dispersion coefficients are given in Table 1.

The response function for the optical pulses is $R(t) = (1 - f_R)\delta(t) + f_R h_R(t)$. The first and second terms represent contributions of the instantaneous electronic and Raman, respectively. Compared with

Table 1. Dispersion coefficients β_n used in our simulation.

β_2 (ps^2/m)	1.44259×10^{-1}	β_8 (ps^8/m)	7.8084×10^{-13}
β_3 (ps^3/m)	-2.14304×10^{-4}	β_9 (ps^9/m)	1.2557×10^{-14}
β_4 (ps^4/m)	1.84391×10^{-6}	β_{10} (ps^{10}/m)	-7.5185×10^{-16}
β_5 (ps^5/m)	6.3906×10^{-9}	β_{11} (ps^{11}/m)	-1.2937×10^{-17}
β_6 (ps^6/m)	-7.36882×10^{-10}	β_{12} (ps^{12}/m)	6.2507×10^{-19}
β_7 (ps^7/m)	-1.125×10^{-11}	β_{13} (ps^{13}/m)	1.1841×10^{-20}

the fused silica material, the Raman contributions are mainly due to the molecular reorientation, which is induced by the tendency of molecules to align in the electric field of the applied optical wave [20]. The fractional contribution of the Raman response f_R is as large as 0.89, and the normalized Raman response function $h_R(t)$ can be written [22] as following,

$$\begin{aligned} h_R(t) \;=\; & 0.5048\exp\left(-\frac{t}{\tau_{\text{diff}}}\right)\left(1-\exp\left(-\frac{t}{\tau_{\text{rise}}}\right)\right) \\ & +0.8314\exp\left(-\frac{t}{\tau_{\text{int}}}\right)\left(1-\exp\left(-\frac{t}{\tau_{\text{rise}}}\right)\right)+1.633\exp\left(-\frac{\alpha^2t^2}{2}\right)\sin\left(\omega_0 t\right) \end{aligned} \tag{6}$$

where $\tau_{\text{diff}} = 1.68\,\text{ps}$, $\tau_{\text{rise}} = 0.14\,\text{ps}$, $\tau_{\text{int}} = 0.4\,\text{ps}$, $\alpha = 5.4/\text{ps}$ and $\omega_0 = 6.72/\text{ps}$.

Coherence is an important parameter for measuring the quality of the generated SC. To simulate the spectral coherence, the random noise with 1% of the pulse intensity is added to the input pump pulses. The complex degree of first-order coherence at each wavelength can be defined [28] as following:

$$\left|g_{12}^{1}\left(\lambda, t_1-t_2\right)\right| = \left|\frac{\left\langle E_1^*\left(\lambda,t_1\right)E_2\left(\lambda,t_2\right)\right\rangle}{\left[\left\langle\left|E_1\left(\lambda,t\right)\right|^2\right\rangle\left\langle\left|E_2\left(\lambda,t\right)\right|^2\right\rangle\right]^{1/2}}\right| \tag{7}$$

where $E_1(\lambda)$ and $E_2(\lambda)$ are the output spectrum from the fiber. The angular brackets denote an ensemble average over independently generated pairs of SC spectra, which are obtained from 100 simulation results. The values of $|g_{12}^1(\lambda)|$ at each wavelength are between 0 and 1.

3. NUMERICAL RESULTS AND DISCUSSION

In this paper, the split-step Fourier transform methods have been used to solve the generalized nonlinear Schrodinger Equation with Runge-Kutta algorithm [26]. In order to understand the mechanism of SC generation which takes place in normal dispersion regime of designed LCPCF, we firstly simulate the temporal and spectral evolutions of the pump pulses along the fiber. In our simulation, the hyperbolic secant pulses at 1550 nm with the peak power of 2 kW and full width at half maximum (FWHM) of 500 fs are used as the pump.

Figures 3(a) and 3(b) show the temporal and spectral evolutions of the pump pulses along the LCPCF. It can be seen that the pump pulses are gradually compressed, and the corresponding optical spectra are asymmetrically broadened toward the shorter and longer wavelengths as the propagation distance increases. During this process, splitting of the pulse and spectrum occurs. To further understand the nonlinear evolutions, the output pulses and spectra for different propagation lengths are shown in Figs. 3(c) and 3(d). Because of the large Raman contribution in the response function of CS_2, the lower frequency components are efficiently generated by the combination of the Raman and SPM effects. At the propagation distance (L) of 0.025 m, the SC spanning from 1445 to 1790 nm is generated. Due to the faster propagation velocity of the lower instantaneous frequency components generated in the normal dispersion region, they are gradually shifted to the forward tail of the pulses. With the accumulation of nonlinear effect, the lower frequency components are enhanced by the SPM and Raman effects. In the time domain, the increase of energy on the leading edges results in the pulse splitting for $L = 0.04$ and 0.05 m. And output spectrum also splits into two parts. When $L = 0.1$ m, SC spanning from 1355 to 2110 nm can be obtained, and the -40 dB bandwidth can be up to 755 nm. As the pulses are compressed, the pulse splitting dominates the nonlinear optical process, and several small splitting parts emerge between the two primary parts of the pulses. In the frequency region, these splitting parts show the complex and oscillatory spectral structure. Fig. 4 clearly shows the output spectra (a) and coherence (b) when the propagation length L is 0.1 m. We can see that SC spanning 1355–2110 nm generated and output spectra presents highly oscillatory from 1600 to 1800 nm. And the coherence discussed below is nearly 1.

Next, the spectral width and coherence of SC for different propagation lengths are shown in Figs. 5(a) and 5(b), respectively. With the increase of the fiber length, the output spectral width gradually increases. The spectral bandwidths are 291, 576, 671, 755, and 823 nm for the propagation distance (L) of 0.02, 0.05, 0.07, 0.1, and 0.15 m, respectively. Although it is expected that a wider SC

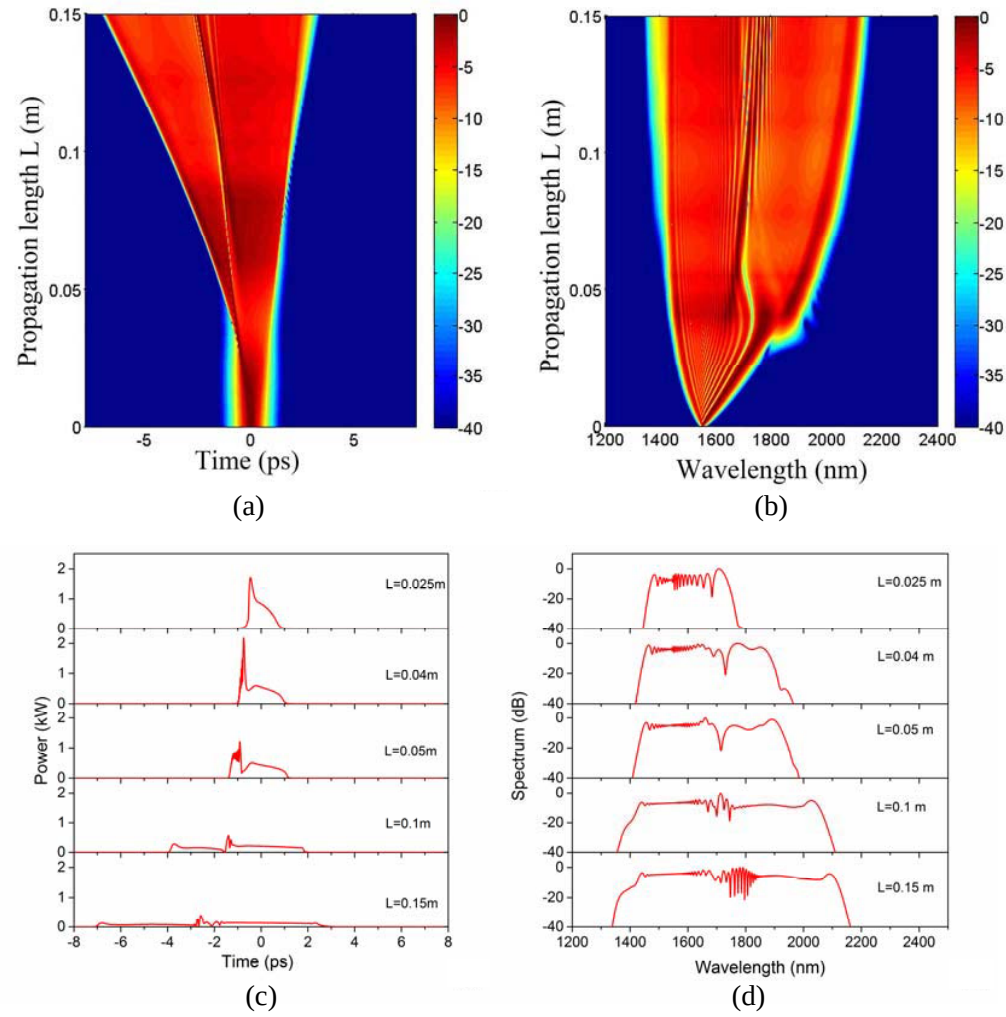

Figure 3. (a) Temporal and (b) spectral evolution of the pump pulses propagated inside the LCPCF, and the output (c) pulses and (d) spectra for different fiber lengths.

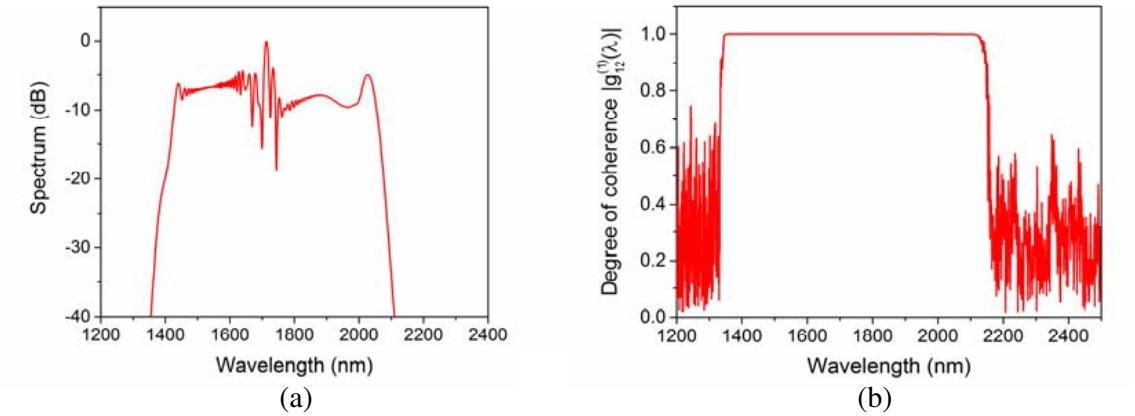

Figure 4. (a) Output spectra and (b) coherence of SC when the propagation length L is 0.1 m.

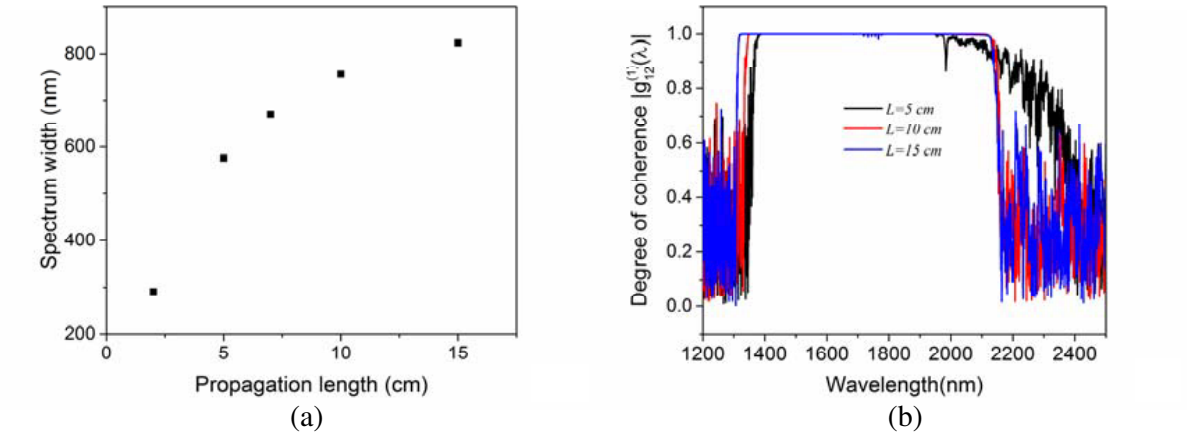

Figure 5. (a) Spectral width and (b) coherence of SC for different fiber lengths.

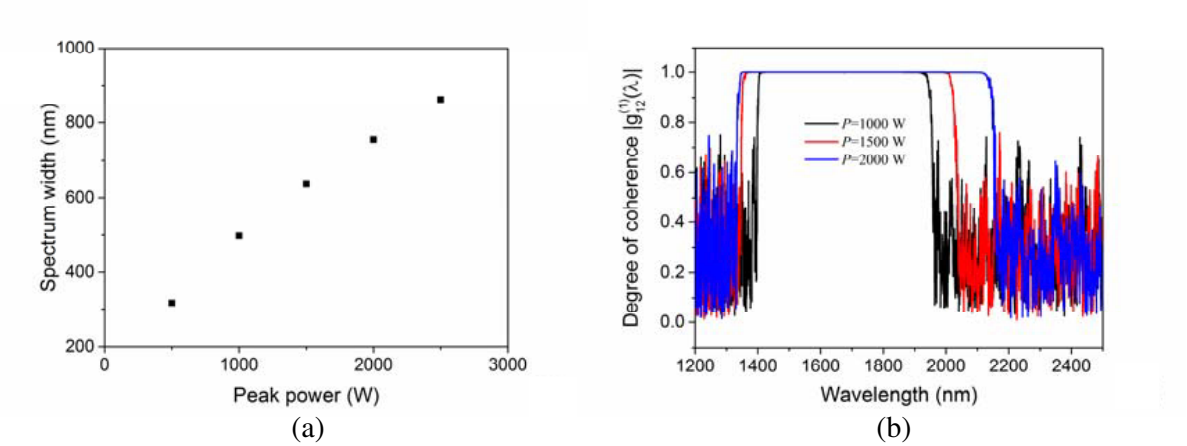

Figure 6. (a) Spectral width and (b) coherence of SC for different pump peak powers.

can be obtained by increasing fiber length, the coherence of SC will become worse, as shown in Fig. 5(b). When $L = 0.05$ m, a dip occurs in the middle of SC induced by the pulse splitting as shown in Fig. 3(d), but the spectral density has a relatively high value. Therefore, the coherence degree of generated SC (calculate from the -40 dB bandwidth) is nearly 1. As the propagation distances are increased, the spectral densities in the dips are relatively low, so the signal-noise ratios are greatly deteriorated when the input background noise and the spontaneous Raman scattering are considered. It is inevitable that the coherence in these dips will get worse with the accumulation of Raman effect. Fig. 5(b) shows that several small defects appear in the middle of spectra spanning from 1750 to 1800 nm at the propagation distance of 0.15 m, which correspond to the oscillatory structure of SC.

The effects of the pump peak power on the spectral width and coherence are also studied when the pump pulses with the duration of 500 fs are launched into the 10 cm-long fiber. From Fig. 6(a) we can see that as the pump peak power increases, the SC widths are greatly broadened. And the spectral bandwidths are 317, 499, 637, 755, and 863 nm for the pump power (P) of 500, 1000, 1500, 2000, and 2500 W, respectively. Fig. 6(b) shows the coherences for $P = 1000$, 1500, and 2000 W. We can see that generated SCs keep perfect (close to 1) coherence as the pump peak power changes.

Due to the large Raman response of CS_2, the SC generation in the designed LCPCF highly depends on the duration of the pump pulses. For the 10 cm-long LCPCF and pump peak power of 2 kW, the pulse duration (T_0) is changed from 250 fs to two ps. Spectral broadening, caused by the Raman effect, is a time accumulation process by the combination of the Raman response and pulse intensity [8]. For an input short pulse, the temporal Raman response contributes less to the nonlinear spectral

broadening [29]. When T_0 is increased, the contribution of the Raman response increases. However, the decreasing bandwidth of the pump pulses as T_0 increases will limit the process of the spectral broadening. As shown in Fig. 7, the generated spectral bandwidths are 632, 755, 775, 790, 767, 724, 700, and 632 nm for the pump pulse duration (T_0) of 250, 500, 750, 1000, 1250, 1500, 1750, and 2000 fs, respectively. It can be seen that the spectral width of SC increases with wider pump pulse duration until $T_0 = 1000$ fs, and the maximal spectral width is up to 790 nm. After that, a decreasing tendency emerges.

In addition, the pulse duration also has a great effect on the output spectrum and coherence of

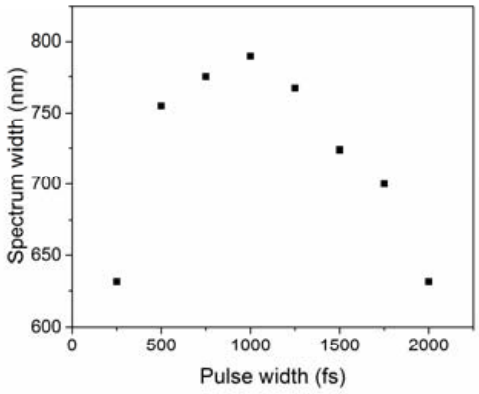

Figure 7. Spectral width of SC for different pulse durations.

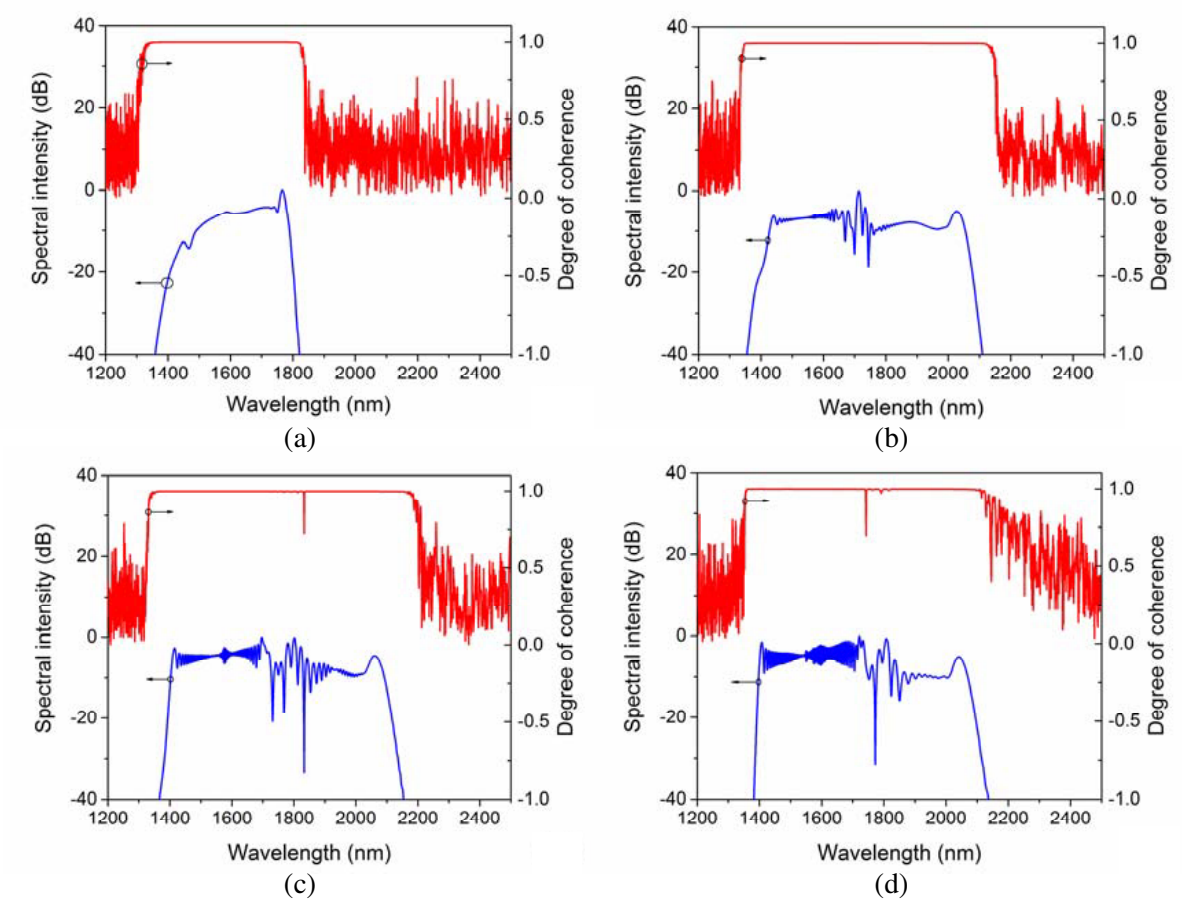

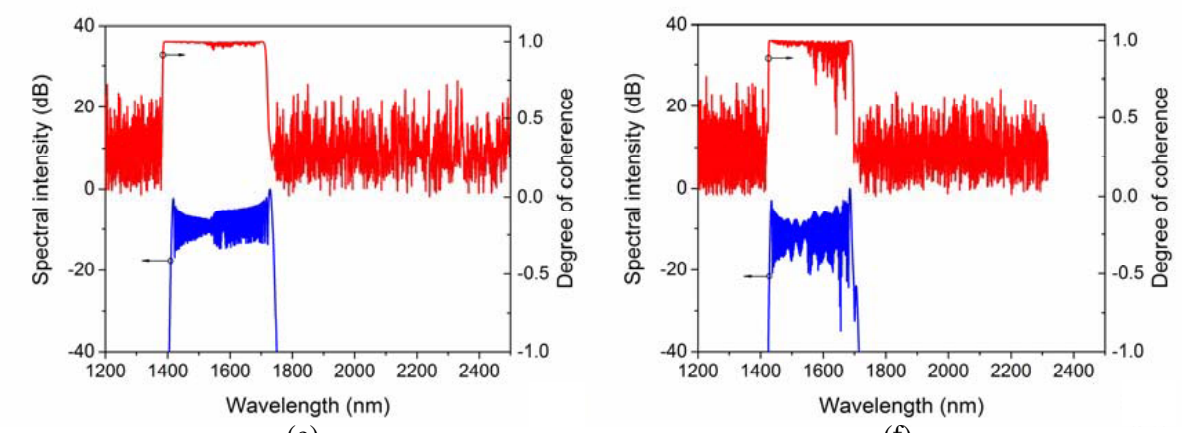

Figure 8. Coherence and output spectra of SC for different pulse durations, (a) 100 fs, (b) 500 fs, (c) 1000 fs, (d) 2000 fs, (e) 4000 fs, and (f) 6000 fs, respectively.

SC. In Fig. 8, output spectra (red lines) and coherence (blue lines) of generated SC for different pulse durations are shown. It is obvious that with the increase of pulse duration, the coherence of generated SC get worse. The Raman effect has greater influence on the spectral broadening than the SPM. For the pump pulses with the shorter duration, the Raman gain mainly takes place on the existing spectral components. Thus, the amplified quantum noise is low compared with the intensity of existing spectral components, and the difference of SC profile generated by each pulse of pulse-series is little [30]. As shown in Figs. 8(a) and 8(b), when the pulse duration is shorter, the coherence degree is close to 1, which represents perfect coherence. The results of Figs. 8(c) and 8(d) can be explained by the nonlinear dynamics mentioned above. With the increase of the pulse durations, the Raman effect can be enhanced, the pulse splitting takes place, and the coherence in dips of SC is degraded. Longer input pulse duration means narrower bandwidth. As the pulse duration increases, the Raman gain then occurs outside the initial pulse bandwidth. So the new spectral components caused by Raman effect will be affected seriously by the amplified quantum noise [30]. The coherence degree will become very poor, as shown in Figs. 8(e) and 8(f).

4. CONCLUSION

In summary, a LCPCF with nonlinear coefficient of $3327\,\mathrm{W^{-1}\cdot km^{-1}}$ at 1550 nm and wide normal dispersion regime spanning from 1200 to 2500 nm is designed for SC generation. The influences of the pump pulse parameters on bandwidth and coherence of the generated SC are studied. This research can determine the optimum pump conditions for the SC generation in such fibers. Simulation results show that highly coherent supercontinuum spanning from 1355 to 2110 nm can be obtained by using 10 cm-long PCF and the 500 fs pump pulses at 1550 nm with the peak power of 2 kW. Therefore, the design LCPCF and pump pulse parameters for SC generation are feasible. Our study work can provide an alternative way for obtaining highly coherent SC, which is important for the applications in optical coherence tomography, frequency combs, and ultrashort pulse generation.

ACKNOWLEDGMENT

This work is partly supported by the National Natural Science Foundation of China (61307109, 61475023, and 61475131), the Beijing Youth Top-notch Talent Support Program (2015000026833ZK08), the Natural Science Foundation of Beijing (4152037), the Fund of State Key Laboratory of Information Photonics and Optical Communications (Beijing University of Posts and Telecommunications) P. R. China (IPOC2015ZC06), the Hong Kong Scholars Program 2013 (PolyU G-YZ45), and the Research Grant Council of the Hong Kong Special Administrative Region China (PolyU5272/12E).

REFERENCES

1. Kaminski, C. F., R. S. Watt, A. D. Elder, et al., "Supercontinuum radiation for applications in chemical sensing and microscopy," *Applied Physics B*, Vol. 92, No. 3, 367–378, 2008.
2. Nakasyotani, T., H. Toda, T. Kuri, et al., "Wavelength-division-multiplexed millimeter-waveband radio-on-fiber system using a supercontinuum light source," *Journal of Lightwave Technology*, Vol. 24, No. 1, 404, 2006.
3. Morioka, T., K. Mori, S. Kawanishi, and M. Saruwatari, "Multi-WDM-channel GBit/s pulse generation from a single laser source utilizing LD-pumped supercontinuum in optical fibers," *IEEE Photonics Technology Letters*, Vol. 6, No. 3, 365–368, 1994.
4. Takara, H., T. Ohara, K. Mori, et al., "More than 1000 channel optical frequency chain generation from single supercontinuum source with 12.5 GHz channel spacing," *Electronics Letters*, Vol. 36, No. 25, 2089–2090, 2000.
5. Moon, S. and D. Y. Kim, "Ultra-high-speed optical coherence tomography with a stretched pulse supercontinuum source," *Optics Express*, Vol. 14, No. 24, 11575–11584, 2006.
6. Udem, T., R. Holzwarth, and T. W. Hänsch, "Optical frequency metrology," *Nature*, Vol. 416, No. 6877, 233–237, 2002.
7. Jones, D. J., S. A. Diddams, J. K. Ranka, et al., "Carrier-envelope phase control of femtosecond mode-locked lasers and direct optical frequency synthesis," *Science*, Vol. 288, No. 5466, 635–639, 2000.
8. Agrawal, G. P., *Nonlinear Fiber Optics*, 4th edition, 2007.
9. Ranka, J. K., R. S. Windeler, and A. J. Stentz, "Visible continuum generation in air-silica microstructure optical fibers with anomalous dispersion at 800 nm," *Optics Letters*, Vol. 25, No. 1, 25–27, 2000.
10. Omenetto, F. G., N. A. Wolchover, M. R. Wehner, et al., "Spectrally smooth supercontinuum from 350 nm to 3 μm in sub-centimeter lengths of soft-glass photonic crystal fibers,". *Optics Express*, Vol. 14, No. 11, 4928–4934, 2006.
11. Qin, G., X. Yan, C. Kito, et al., "Supercontinuum generation spanning over three octaves from UV to 3.85 μm in a fluoride fiber," *Optics Letters*, Vol. 34, No. 13, 2015–2017, 2009.
12. Gu, X., M. Kimmel, A. Shreenath, et al., "Experimental studies of the coherence of microstructure-fiber supercontinuum," *Optics Express*, Vol. 11, No. 21, 2697–2703, 2003.
13. Genty, G., S. Coen, and J. M. Dudley, "Fiber supercontinuum sources," *JOSA B*, Vol. 24, No. 8, 1771–1785, 2007.
14. Hooper, L. E., P. J. Mosley, A. C. Muir, et al., "Coherent supercontinuum generation in photonic crystal fiber with all-normal group velocity dispersion," *Optics Express*, Vol. 19, No. 6, 4902–4907, 2011.
15. Li, P., L. Shi, and Q.-H. Mao, "Supercontinuum generated in all-normal dispersion photonic crystal fibers with picosecond pump pulses," *Chinese Physics B*, Vol. 22, No. 7, 074204, 2013.
16. Yan, P., R. Dong, G. Zhang, et al., "Numerical simulation on the coherent time-critical 2–5 μm supercontinuum generation in an As2S3 microstructured optical fiber with all-normal flat-top dispersion profile," *Optics Communications*, Vol. 293, 133–138, 2013.
17. Hartung, A., A. M. Heidt, and H. Bartelt, "Design of all-normal dispersion microstructured optical fibers for pulse-preserving supercontinuum generation," *Optics Express*, Vol. 19, No. 8, 7742–7749, 2011.
18. Poli, F., A. Cucinotta, S. Selleri, et al., "Tailoring of flattened dispersion in highly nonlinear photonic crystal fibers," *IEEE Photonics Technology Letters*, Vol. 16, No. 4, 1065–1067, 2004.
19. Saitoh, K. and M. Koshiba, "Highly nonlinear dispersion-flattened photonic crystal fibers for supercontinuum generation in a telecommunication window," *Optics Express*, Vol. 12, No. 10, 2027–2032, 2004.
20. Bozolan, A., C. J. de Matos, C. Cordeiro, et al., "Supercontinuum generation in a water-core photonic crystal fiber," *Optics Express*, Vol. 16, No. 13, 9671–9676, 2008.

21. Zhang, H., S. Chang, J. Yuan, et al., "Supercontinuum generation in chloroform-filled photonic crystal fibers," *Optik-International Journal for Light and Electron Optics*, Vol. 121, No. 9, 783–787, 2010.
22. Zhang, R., J. Teipel, and H. Giessen, "Theoretical design of a liquid-core photonic crystal fiber for supercontinuum generation," *Optics Express*, Vol. 14, No. 15, 6800–6812, 2006.
23. Kedenburg, S., T. Gissibl, T. Steinle, et al., "Towards integration of a liquid-filled fiber capillary for supercontinuum generation in the 1.2–2.4 μm range," *Optics Express*, Vol. 23, No. 7, 8281–8289, 2015.
24. Churin, D., T. N. Nguyen, K. Kieu, et al., "Mid-IR supercontinuum generation in an integrated liquid-core optical fiber filled with CS2," *Optical Materials Express*, Vol. 3, No. 9, 1358–1364, 2013.
25. Yiou, S., P. Delaye, A. Rouvie, et al., "Stimulated Raman scattering in an ethanol core microstructured optical fiber," *Optics Express*, Vol. 13, No. 12, 4786–4791, 2005.
26. Cox, F. M., A. Argyros, and M. C. J. Large, "Liquid-filled hollow core microstructured polymer optical fiber," *Optics Express*, Vol. 14, No. 9, 4135–4140, 2006.
27. Hult, J., "A fourth-order Runge-Kutta in the interaction picture method for simulating supercontinuum generation in optical fibers," *Journal of Lightwave Technology*, Vol. 25, No. 12, 3770–3775, 2007.
28. Dudley, J. M., G. Genty, and S. Coen, "Supercontinuum generation in photonic crystal fiber," *Reviews of Modern Physics*, Vol. 78, No. 4, 1135, 2006.
29. Klimczak, M., G. Soboń, K. Abramski, et al., "Spectral coherence in all-normal dispersion supercontinuum in presence of Raman scattering and direct seeding from sub-picosecond pump," *Optics Express*, Vol. 22, No. 26, 31635–31645, 2014.
30. Zaitsu, S., Y. Kida, and T. Imasaka, "Stimulated Raman scattering in the boundary region between impulsive and nonimpulsive excitation," *JOSA B*, Vol. 22, No. 12, 2642–2650, 2005.